

Third Nearest WZ Sge-Type Dwarf Nova candidate ASASSN-14dx Classified on the Basis of Gaia Data Release 2

Keisuke ISOGAI,^{1*} Taichi KATO,¹ Akira IMADA,^{2,3} Tomohito OHSHIMA,⁴
Naoto KOJIGUCHI,¹ Ryuhei OHNISHI,¹ Franz-Josef HAMBSCH,^{5,6,7}
Berto MONARD,⁸ Seiichiro KIYOTA,⁹ Hideo NISHIMURA,¹⁰ Daisaku NOGAMI¹

¹ Department of Astronomy, Kyoto University, Kyoto 606-8502

² Hamburger Sternwarte, Universität Hamburg, Gojenbergsweg 112, D-21029
Hamburg, Germany

³ Kwasan and Hida Observatories, Kyoto University, Yamashina, Kyoto 607-8471

⁴ Nishi-Harima Astronomical Observatory, University of Hyogo, Japan

⁵ Groupe Européen d'Observations Stellaires (GEOS), 23 Parc de Levesville, 28300 Bailleau l'Evêque, France

⁶ Bundesdeutsche Arbeitsgemeinschaft für Veränderliche Sterne (BAV), Munsterdamm 90,
12169 Berlin, Germany

⁷ Vereniging Voor Sterrenkunde (VVS), Oude Bleken 12, 2400 Mol, Belgium

⁸ Bronberg and Kleinkaroo Observatories, Center for Backyard Astrophysics Kleinkaroo, Sint
Helena 1B, PO Box 281, Calitzdorp 6660, South Africa

⁹ VSOLJ, 7-1 Kitahatsutomi, Kamagaya, Chiba 273-0126, Japan

¹⁰ Miyawaki 302-6, Kakegawa, Shizuoka 436-0086, Japan

*E-mail: *isogai@kusastro.kyoto-u.ac.jp

Received 201 0; Accepted 201 0

Abstract

ASASSN-14dx showed an extraordinary outburst whose features are the small outburst amplitude (~ 2.3 mag) and long duration (> 4 years). Because we found a long observational gap of 123 d before the outburst detection, we propose that the main outburst plateau was missed and that this outburst is just a “fading tail” often seen after the WZ Sge-type superoutbursts. In order to distinguish between WZ Sge and SU UMa-type dwarf novae (DNe), we investigated *Gaia* DR2 statistically. We applied a logistic regression model and succeeded in classifying by using absolute *Gaia* magnitudes M_G and *Gaia* colors $G_{\text{BP}} - G_{\text{RP}}$. Our new classifier also suggests that ASASSN-14dx is the best candidate of a WZ Sge-type DN. We estimated distances from the Earth of known WZ Sge stars by using *Gaia* DR2 parallaxes. The result indicates that ASASSN-14dx is the third nearest WZ Sge star (next to WZ Sge and V455 And), and hence the object can show the third brightest WZ Sge-type superoutburst whose maximum is $V = 8\text{--}9$ mag.

Key words: accretion, accretion disks — stars: novae, cataclysmic variables — stars: dwarf novae, WZ Sge — stars: individual (ASASSN-14dx)

1 Introduction

Cataclysmic variables (CVs) are close binaries composed of a white dwarf (WD) primary and a Roche lobe-filling secondary. An accretion disk is formed around the primary because the secondary transfers its mass to the primary. Dwarf Novae (DNe), which are a subclass of CVs, are characterized by a sudden increase of the disk brightness called “outburst”. There are two competing models to explain a dwarf nova outburst: the mass-transfer burst model (Bath 1973) and the thermal instability model (Osaki 1974; Hōshi 1979). At the present time, the latter is widely accepted at least for typical dwarf nova outbursts. For instance, Dubus et al. (2018) estimated the mass-transfer rates of 130 CVs by using the parallax distances of the *Gaia* Data Release 2 (DR2). The estimated mass-transfer rates of dwarf novae and nova-like stars are consistent with their theoretical values predicted by the thermal instability model, respectively. (for a review of CVs and DNe, see e.g. Warner 1995).

SU UMa-type DNe show not only normal outbursts but also superoutbursts with larger scales. During superoutbursts, we can observe “superhumps” whose amplitude is 0.1–0.5 mag and period is a few percent longer than the orbital period P_{orb} . Superoutbursts and superhumps are thought to be a result of the thermal-tidal instability (Osaki 1989). When an outburst begins, the disk expands. If the object has a sufficiently low mass ratio q , the outer edge of the disk can reach the 3:1 resonance radius which causes the tidal instability (Whitehurst 1988; Osaki 1989; Lubow 1991a; Lubow 1991b; Hirose, Osaki 1990).

WZ Sge-type DNe are a subclass of SU UMa-type ones and considered to be objects at the terminal stage of the CV evolution. WZ Sge stars are characterized by the large amplitude and long duration superoutbursts which are accompanied by “early superhumps” in the early terms of the superoutbursts. According to the modern criteria provided by Kato (2015), WZ Sge stars are defined by the presence of an early superhump phase. It is thought that early superhumps are triggered by the 2:1 resonance (Lin, Papaloizou 1979; Osaki, Meyer 2002). Early superhumps are double-peaked modulations whose periods are close to P_{orb} . Because the early superhumps are caused by a geometrical effect, their amplitudes depend on their inclination angles. Thus, in low-inclination systems, we can observe a long outburst plateau with no superhumps instead of an early superhump phase. SU UMa stars evolve into WZ Sge ones as the mass transfer proceeds because only CVs with extremely low mass ratios (typically $q < 0.09$) and low mass-transfer rates can reach the 2:1 resonance radius, (for a review of WZ Sge-type DNe, see Kato 2015).

According to the theoretical CV evolution calculated by Kolb (1993), 70% of CVs have already passed the period minimum. Such objects are called “period bouncers”. The secondary masses of the period bouncers are below the substellar limit. Their q and mass-transfer rates are thus extremely low as compared with DNe before the period minimum. Empirically, we know many objects around the period minimum show WZ Sge-type superoutbursts. These facts imply that most of DNe are WZ Sge stars. However, the number of WZ Sge stars is much smaller than that of SU UMa ones. The gap between the theory and observation can be caused by the observational bias because WZ Sge stars are fainter and their outburst intervals are longer in comparison to SU UMa ones. Thus, it is important to dig up the hidden WZ Sge stars. In addition, there are some unsolved problems in WZ Sge stars, e.g. the detailed mechanism of early superhumps or rebrightenings. The increasing number of WZ Sge stars will give us more opportunities to observe such phenomena.

We report on the outburst and classification of ASASSN-14dx. The outburst was detected at $V = 13.95$ on June 25, 2014 by the All-Sky Automated Survey for Supernovae (ASAS-SN) (Shappee et al. 2014). The coordinates are RA = 02:34:27.73 and Dec = -04:54:30.7 at J2000.0. The Sloan Digital Sky Survey (SDSS) magnitudes are $u = 16.42, g = 16.26, r = 16.37, i = 16.55, z = 16.63$ (Ahn et al. 2012). The object is an XMM-Newton source and has a GALEX counterpart with an NUV and FUV magnitudes of 16.4 and 16.6 (Martin et al. 2005). The spectra were obtained in August 2014 (Kaur et al. 2014) and in October 2014 (Thorstensen et al. 2016). They reported double-peaked emission lines with broad and narrow absorption ones on a blue continuum, and thus the object was confirmed as a CV. Since follow-up photometries by our group and Hardy et al. (2017) reported the superhump-like modulations, the object was initially classified as an SU UMa star. Hardy et al. (2017) confirmed that the object doesn’t show any eclipses. On the basis of our light curve analyses and new classification method by using the *Gaia* Data Release 2 (DR2) (Gaia Collaboration et al. 2016; Gaia Collaboration et al. 2018b), we propose that ASASSN-14dx is a WZ Sge star rather than SU UMa one.

2 Observation and Analysis

Our time-series observations are summarized in table E1. The data were acquired by time-resolved unfiltered CCD photometry using 30–40cm class telescopes by the VSNET Collaboration (Kato et al. 2004). The times of the observations were corrected to Barycentric Julian Date (BJD).

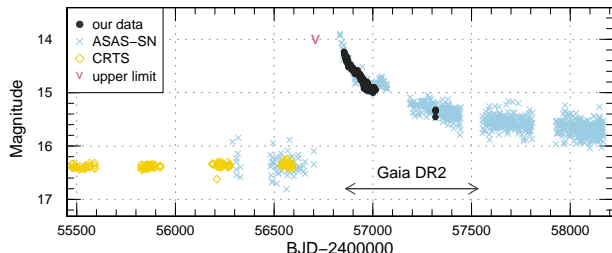


Fig. 1. Overall light curves of ASASSN-14dx. Filled circles, crosses, open diamonds and “V”-mark represent our observations, the ASAS-SN data, the CRTS data and the upper limit, respectively. Our time-series observations were binned to 0.01 d. The observation period of *Gaia* DR2 is indicated by the arrows.

We adjusted the zero-point of each observer to Franz-Josef Hambisch’s data.

We used the phase dispersion minimization (PDM) method for analyzing the periodic modulations. We estimated 1σ errors by using the methods in Fernie (1989) and Kato et al. (2010). Before our period analyses, we subtracted the global trend of the light curve which was calculated by using locally-weighted polynomial regression (LOWESS, Cleveland 1979).

3 Results

3.1 Overall Light Curve

Figure 1 shows the overall light curve of ASASSN-14dx. The light curve also includes the public data of the CRTS (Drake et al. 2009) and ASAS-SN Sky Patrol (Shappee et al. 2014; Kochanek et al. 2017). Before the outburst, the object was stable around $V = 16.36$ mag. The outburst was detected at $V = 13.95$ mag on June 25, 2014 (BJD 2456833), then the object gradually decreased to $V \sim 15.7$ mag until 2018. Such a small-amplitude and long-duration outburst is very unusual for DN outbursts.

We found an upper limit of 14.0 mag on February 22, 2014 (BJD 2456710) indicated in figure 1 as “V”-mark. After this observation, we don’t have any data until the outburst detection due to seasonal reason, namely, there is a long observational gap of 123 d. This gap implies that we missed the initial phase of the outburst and that this outburst is just a “fading tail”.

A fading tail is a well-known phenomenon seen after WZ Sge-type superoutbursts. Specifically, Kuulkers et al. (2011) reported the moderate declines of WZ Sagittae after the end of the superoutbursts plateau. The brightness just after the superoutbursts is about 0.5 mag brighter than in quiescence. They proposed that the decline can be caused by the development of a cavity in the inner disk and that the time scale is about a decade. For another example,

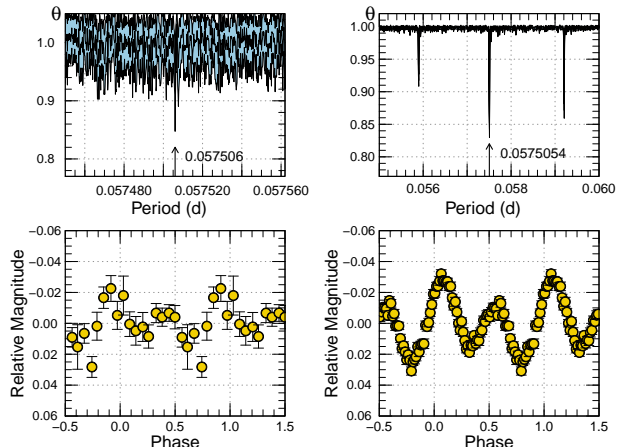


Fig. 2. Results of the period analyses of orbital modulations in quiescence (BJD 2453627.89–2456591.85) (Left) and outburst (BJD 2456854.82–2457014.09) (Right). (Upper): θ diagram of our PDM analysis of superhumps. The shaded area means 1σ errors. (Lower): Phase-averaged profiles of orbital modulations. The zero phases were defined to be BJD 2456945.8837, which is the time of the inferior conjunction obtained by Thorstensen et al. (2016).

SSS J122221.7-311523 (hereafter J1222) showed a fading tail lasting at least 500 d and the brightness just after the superoutburst is about 3 mag brighter (Neustroev et al. 2017). The outburst profile of ASASSN-14dx is in good agreement with them rather than ordinary outbursts.

3.2 Double-wave modulations

During the outburst, the object showed persistent double-wave modulations. The result of the period analysis of our observations in BJD 2456854.82–2457014.09 is indicated in figure 2. The estimated period is 0.0575054(4) d. The interval of two peaks is nearly 0.5 phase. Since the modulations were initially interpreted as superhumps, the object was classified as an SU UMa-type DN (cf. vsnet-alert 17598, Hardy et al. 2017).

4 Discussion

4.1 Orbital Modulations

The left panel of figure 2 shows the period analysis of the CRTS data in quiescence (BJD 2453627.89–2456591.85). We reported a weak signal of a possible orbital period of 0.0575060(2) d (vsnet-alert 18017). Thorstensen et al. (2016) estimated the orbital period to be 0.05756(6) d from H α radial velocities via spectroscopy, and they confirmed that this value is consistent with our result. These values are close to the period detected during the outburst of 0.0575054(4) d. The averaged profiles are also similar to each other (the lower panels in figure 2). Thus we propose

that the modulations in the outburst are not superhumps but orbital modulations. We adopted the period in quiescence of $0.0575060(2)$ d as the orbital one because of the small error and the long baseline of the data.

WZ Sge-type DNe, especially in high-inclination systems, often show double-wave orbital modulations in quiescence or fading tail (e.g. Patterson et al. 1996). Skidmore et al. (2000) investigated the disk structure of WZ Sagittae in quiescence from the Doppler mapping. They found that the bright spot exists along the ballistic trajectory, and considered that a low-density disk allows accretion stream to penetrate and thus can explain double-wave modulations originated from the change of the line-of-sight. Kononov et al. (2015) simulated the humps of WZ Sge stars by using the three-dimensional computation. They proposed that a spiral density wave and four kinds of shocks can cause such modulations. Because the density wave undergoes a slow retrograde precession in the observer's frame and the interaction between the density wave and four shocks generates the modulations, they succeeded in reproducing the profile variations and phase shifts of humps, which are sometimes seen in WZ Sge stars. Note that the period of such humps can be shorter than the orbital one in a strict sense. The modulations of ASASSN-14dx could also be explained by these mechanisms.

The estimated period of ASASSN-14dx in the outburst is very slightly shorter than that in quiescence. According to the thermal instability model, a disk after an outburst gradually shrinks due to the accreting mass (cf. Osaki 1989). Shrinkage of a disk could lead to a phase shift of the modulations, e.g. a shift of the position of the bright spot. In principle, we cannot discriminate between a continuous phase shift and a period variation. On the other hand, the model of Kononov et al. (2015) can account for the shorter period owing to the change of the precession rate of the density wave. The small difference in the periods might be caused by these varying disk structure.

We drew the averaged profiles of orbital modulations (the lower panels of figure 2). We estimated the time of the inferior conjunction, the secondary star is the closest to the Earth, to be BJD 2456945.8837(7) on the basis of the time-resolved spectroscopies obtained by Thorstensen et al. (2016), and we defined the zero phases to be BJD 2456945.8837. For the purpose of understanding the mechanism of the humps, it may be worth mentioning that both of the peaks of the modulations are close to the conjunction. However, we must note that the time of the conjunction is estimated by using the disk emissions, whose light source is unclear. Therefore this value has an uncertainty, and we need to observe lines from the secondary star to obtain the accurate time of the conjunction. These

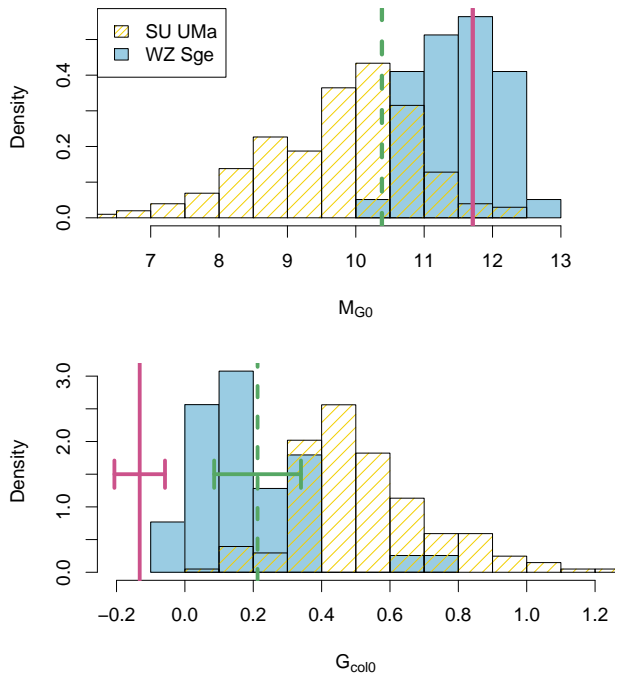


Fig. 3. Density distributions of corrected absolute *Gaia* magnitudes M_{G0} (upper) and *Gaia* colors $G_{\text{col}0}$ (lower). Hatched and shaded boxes represent SU UMa and WZ Sge-type DNe, respectively. Solid and dashed vertical lines indicate ASASSN-14dx in the SDSS (quiescence) and *Gaia* DR2 (outburst), respectively. The error bars of ASASSN-14dx are shown only in the lower panel because of the large errors. We removed three WZ Sge-type DN candidates mentioned in section 4.3.

figures suggest that the phases of the peaks in quiescence and outburst are respectively $-0.06(2)$ and $0.08(1)$, namely the object showed a phase shift of $0.14(2)$. Note that the folding periods are different from each other. However, even if we fold the light curve in outburst by using the period in quiescence, the phase is little varied (less than 0.01 phase). It may be difficult to explain the large shift only by a simple bright spot and shrinking disk, while the model of Kononov et al. (2015) can explain it on the basis of the retrograde-precession density wave.

4.2 Classification by *Gaia* DR2

In order to distinguish WZ Sge stars from SU UMa ones, we investigated the known DNe of the *Gaia* DR2. By using the parallaxes ϖ and three broad band optical magnitudes (white light G , blue G_{BP} and red G_{RP}) provided by the *Gaia*, we can estimate the absolute *Gaia* magnitudes M_G and *Gaia* colors $G_{\text{col}} = G_{\text{BP}} - G_{\text{RP}}$ (Luri et al. 2018; Riello et al. 2018; Evans et al. 2018). Although the *Gaia* team has already studied on the color-absolute magnitude diagram about variable stars (Gaia Collaboration et al. 2018c), we concentrated more on the subclasses of DNe. The CV evolutionary track computed by Knigge et al. (2011) shows

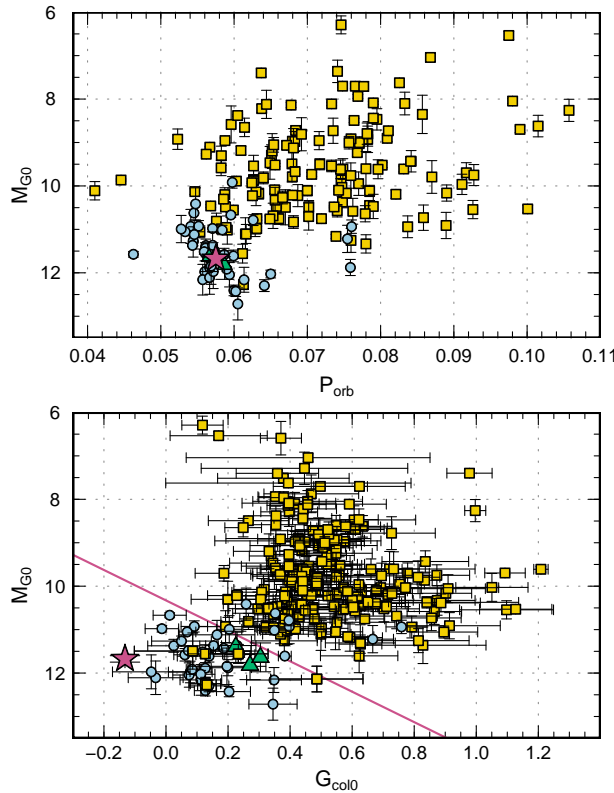


Fig. 4. Corrected absolute *Gaia* magnitude M_{G0} versus orbital period P_{orb} (upper) and *Gaia* color G_{col0} (lower). Regarding WZ Sge-type DNe whose orbital periods are unknown, we estimated the orbital periods from the superhump periods and equation (6) in Kato et al. (2012a). The filled squares, circles and star represent SU UMa, WZ Sge-type DNe and ASASSN-14dx, respectively. Three WZ Sge star candidates mentioned in section 4.3 are shown as filled triangles. The solid line in the lower panel indicates $P_{\text{WZ}} = 0.5$ which means the borderline between SU UMa and WZ Sge stars.

that absolute magnitudes become fainter and that the colors become bluer as CVs evolve. Actually, we can see WZ Sge-type DNe lying on the bluer area in the color-color diagram of the SDSS (Kato et al. 2012b). Furthermore, it is considered that M_G depends also on the mass-transfer rates from secondaries, i.e. the brightness of bright spots and disks (cf. Dubus et al. 2018).

We identified known SU UMa/WZ Sge-type DNe with the *Gaia* DR2 sources. The list of known DNe was taken from the AAVSO VSX¹. We only used objects whose ϖ errors are within 20%. The galactic extinctions in V and B bands (A_V and A_B) for each object were obtained from the NED² (Schlafly, Finkbeiner 2011). Because the galactic extinctions are affected by the positions of the objects, we estimated the effects by using equation 2 in Ak et al.

(2008), the distances d calculated from ϖ and the assumed scale height for the interstellar dust $H = 100$ pc. Then we converted A_V and A_B to the extinctions in *Gaia* magnitudes ($A_G, A_{\text{BP}}, A_{\text{RP}}$) on the basis of equation 1 and table 1 in Gaia Collaboration et al. (2018a). Eventually, we used the corrected absolute magnitudes $M_{G0} = M_G - A_G$, de-reddened colors $G_{\text{col0}} = G_{\text{col}} - (A_{\text{BP}} - A_{\text{RP}})$ and P_{orb} for the statistics. We note that the effects of galactic extinction have large uncertainties and are sometimes neglected (e.g. Gaia Collaboration et al. 2018c). Thus we removed the objects with large extinctions $A_G > 0.5$ in our statistics to suppress the uncertainty.

Figure 3 shows the density distributions of M_{G0} and G_{col0} . Hatched and shaded boxes represent SU UMa and WZ Sge stars, respectively. As expected by previous studies, WZ Sge stars are basically fainter and bluer. These features can give the interpretations that the mass-transfer rate is lower and that the WD's contribution to the color is more important in WZ Sge stars. The upper panel implies that there is a lower limit of $M_{G0} \sim 10.5$ as for WZ Sge stars. This fact is consistent with the interpretation of early superhumps by the TTI model. In other words, a low mass-transfer rate is needed to accumulate enough mass at the onset of an outburst to trigger the 2:1 resonance (Osaki 1995).

ASASSN-14dx is indicated by dashed lines in figure 3. Their positions are a little far from other WZ Sge-type objects. The reason is that the *Gaia* obtained the data during the outburst as indicated in figure 1. In order to estimate the *Gaia* magnitudes in quiescence, we converted the SDSS magnitudes, were observed before the outburst, to *Gaia* ones by using table A.2 in Evans et al. (2018). Then, we obtained the quiescent values of $M_{G0} = 11.71(43)$ and $G_{\text{col0}} = -0.112(74)$ indicated by solid lines in figure 3. These figures give the impression that ASASSN-14dx is indeed a WZ Sge-type DN.

Figure 4 shows the relations between M_{G0} and P_{orb} (upper), and M_{G0} and G_{col0} (lower). The filled squares, circles and star represent SU UMa, WZ Sge-type DNe and ASASSN-14dx in quiescence, respectively. The triangles indicate new WZ Sge-type DN candidates discussed in section 4.3. We removed them from our statistics. Three WZ Sge-type stars around $P_{\text{orb}} \sim 0.076$ d are two long- P_{orb} WZ Sge stars (RZ Leo and ASASSN-16eg) and one period bouncer J1222. Wakamatsu et al. (2017) interpreted the long- P_{orb} WZ Sge stars as borderline objects between SU UMa and WZ Sge-type DNe, which have low mass-transfer rates in spite of their high-mass ratios. They are indeed fainter than other SU UMa stars having similar P_{orb} . On the other hand, their colors are redder in comparison with the other WZ Sge stars (see two objects with G_{col0} of 0.6–

¹ <<https://www.aavso.org/vsx/>>.

² The NASA/IPAC Extragalactic Database (NED) is operated by the Jet Propulsion Laboratory, California Institute of Technology, under contract with the National Aeronautics and Space Administration.

0.8 in the lower panels of figure 3 and 4).

From the lower panel of figure 4, we established a classification method between WZ Sge and SU UMa stars by using a logistic regression model (Verhulst 1845; Verhulst 1847). On the basis of the data in the lower panel, we can estimate the WZ Sge-type DN probability P_{WZ} as a function of M_{G0} and $G_{\text{col}0}$:

$$P_{\text{WZ}} = \frac{1}{1 + \exp(19.8573 + 6.7335G_{\text{col}0} - 1.9227M_{G0})}. \quad (1)$$

The solid line in figure 4 represents $P_{\text{WZ}} = 0.5$. We propose $P_{\text{WZ}} = 0.5$ as the classifier of WZ Sge/SU UMa-type DNe. For the sake of convenience, we obtained the WZ Sge probability without taking the galactic extinctions into account:

$$P'_{\text{WZ}} = \frac{1}{1 + \exp(15.9452 + 7.5695G_{\text{col}} - 1.5448M_G)}. \quad (2)$$

We note that this equation should not be used for high- A_G objects. We provide a sample R code to estimate P_{WZ} and the extinctions on our website³.

We estimated P_{WZ} for each object including large- A_G objects and summarized in table E2 and E3. P_{WZ} of ASASSN-14dx is 0.21(14) in the Gaia DR2 (outburst) but 0.97(1) in the SDSS (quiescence). Our new classifier also suggests that ASASSN-14dx is the best candidate of a WZ Sge star. We evaluated the validity of the $P_{\text{WZ}} = 0.5$ method, then 32 in 41 WZ Sge stars and 219 in 225 SU UMa ones are correctly classified, whereas $P'_{\text{WZ}} = 0.5$ classified 30 WZ Sge ones and 220 SU UMa ones. However, some WZ Sge stars could be classified as SU UMa ones due to the lacking data. Intensive observations for high- P_{WZ} systems will improve our classification method.

4.3 Exploration of WZ Sge-type DN candidates

We concluded that the following three objects are good candidates of WZ Sge-type DNe on the basis of P_{WZ} and the modern criteria provided in Kato (2015):

- PNV J19321040-2052505

The estimated P_{WZ} is 0.63(18). This object was detected on 2017 Nov. 11 by H. Nishimura⁴. A follow-up observation confirmed a possible signal of superhumps, and hence the object was classified as an SU UMa-type DN (vsnet-alert 21694). According to ASAS-3 data, the object showed an outburst in 2003 (Pojmański 2002). The duration of the outburst was longer than 27 days and the outburst amplitude was large ($\sim 8\text{mag}$). These values strongly suggest that the object is a WZ Sge-type DN.

³ <http://www.kusastro.kyoto-u.ac.jp/~isogai/Pwz/>

⁴ <<http://www.cbat.eps.harvard.edu/unconf/followups/J19321040-2052505.html>>.

- CRTS J200331.3-284941

The estimated P_{WZ} is 0.74(19). The ordinary superhumps were detected in the 2015 outburst. Kato et al. (2016) speculated that this object can be a WZ Sge-type DN on the basis of the low mass ratio of 0.084(1), long duration of growing (stage A) superhumps (more than 50 cycles), fading tail like WZ Sge-type DNe and long observational gap.

- ASASSN-17kg

The estimated P_{WZ} is 0.62(17). This object was detected on Jul. 31, 2016 by the ASAS-SN and the last observation before the detection was on Jul. 27 (Shappee et al. 2014). The follow-up observation on Aug. 3 detected growing superhumps (vsnet-alert 21326). In other words, there was an observational gap of seven days. Although the typical duration of the early superhump stage is 10 d or more (Kato 2015), table 9 in Nakata et al. (2013), which listed those of well-observed WZ Sge-type DNe, shows the minimum duration is 5 d. This fact suggests that the observational gap of one week could conceal the early superhump phase. Moreover, the object showed one rebrightening after the superoutburst (vsnet-alert 21360). We thus concluded that this object is a WZ Sge-type DN candidate.

Other SU UMa stars with a long observational gap could also be WZ Sge ones. In future, we should pay attention to high- P_{WZ} objects in order not to miss the early superhump phase. Note that there are some unusual WZ Sge stars. It may be difficult to discover them on the basis of P_{WZ} . Although AL Com was considered to be a typical WZ Sge star, the object showed SU UMa-type superoutburst in 2015 (Kimura et al. 2016). The estimated P_{WZ} of 0.11(19) is indeed low (we removed AL Com from our statistics due to the large error of ϖ). As mentioned in section 4.2, the long- P_{orb} WZ Sge stars (RZ Leo, ASASSN-16eg and BC UMa) have large $G_{\text{col}0}$, and hence the P_{WZ} are less than 0.15. In addition, the Gaia DR2 data are possibly contaminated by outbursts, eclipses and so on like ASASSN-14dx. Therefore, a complete classification based on the Gaia data may be essentially difficult.

4.4 Distances of WZ Sge-type DNe

We calculated the probability distributions of the distances d of known WZ Sge stars by using the Gaia parallaxes ϖ and the method of Bailer-Jones et al. (2018), assumes a Galaxy model. We obtained the median values and the 16th and 84th percentiles of the distributions. Those of nearby object are listed in table 1. ASASSN-14dx seems to be the third nearest WZ Sge-type DN. This fact suggests that the superoutburst maximum of ASASSN-14dx

can reach $V = 8\text{--}9$ mag. Thus ASASSN-14dx is one of the best targets for the observational research of WZ Sge-type DNe.

Table 1. List of nearby WZ Sge-type DNe

Object	d^{\ddagger}	G^{\parallel}
ASASSN-14dx	80.8 [80.6, 81.1]	15.0
WZ Sge	45.1 [45.0, 45.2]	15.2
V455 And	75.4 [75.1, 75.7]	16.1
BW Scl	94.2 [93.3, 95.0]	16.3
V627 Peg	99.4 [98.8, 100.1]	15.7
GW Lib	112.5 [111.4, 113.5]	16.5
EZ Lyn	145.3 [142.1, 148.6]	17.8
V355 UMa	149.6 [147.7, 151.5]	17.4
FL Ps	153.1 [150.0, 156.3]	17.5
V406 Vir	168.8 [164.5, 173.3]	17.7
PNV J1714 *	176.9 [172.5, 181.6]	17.2
EG Cnc	184.9 [175.0, 195.9]	18.8
QZ Lib	189.2 [178.0, 201.9]	18.9
V1838 Aql	201.6 [195.0, 208.7]	17.9
1RXS J0232 *	206.9 [198.8, 215.8]	18.7
OV Boo †	210.5 [204.4, 216.9]	18.2
V624 Peg	217.7 [204.1, 233.2]	18.4
TCP J1815 *	220.0 [208.6, 232.7]	19.2
SSS J1222 *	239.8 [220.5, 262.8]	18.9
PNV J0309 *	246.6 [230.8, 264.6]	18.7
ASASSN-14cl	261.2 [248.9, 274.9]	18.2

† Distance estimated by using the parallax ϖ in *Gaia* DR2 and the method of Bailer-Jones et al. (2018). The left values are the medians of the distance probability distributions, and the right values in the brackets are the 16th and 84th percentiles. Unit of pc.

‡ G magnitude in *Gaia* DR2. Unit of mag.

* PNV J1714 = PNV J17144255-2943481, 1RXS J0232 = 1RXS J023238.8-371812, TCP J1815 = TCP J18154219+3515598, SSS J1222 = SSS J122221.7-311523, PNV J0309 = PNV J03093063+2638031.

† Population II CV below the period minimum which showed a WZ Sge-type superoutburst.

5 Summary

Although ASASSN-14dx was classified as an SU UMa-type DN due to the long observational gap, the object is likely to be the best candidate of a WZ Sge-type one judging from the outburst behavior, *Gaia* absolute magnitude and *Gaia* color. The double-wave modulations observed in the outburst seem to be orbital modulations, are often seen in WZ Sge stars, rather than superhumps. The estimated distances of known WZ Sge stars indicate that ASASSN-14dx

is the third nearest WZ Sge star and that the superoutburst maximum of ASASSN-14dx can reach $V = 8\text{--}9$ mag. ASASSN-14dx is one of the best targets for observational research of WZ Sge stars because such a bright object will give us high S/N data.

We examined a new classification method of WZ Sge/SU UMa-type DNe based on the *Gaia* DR2. The logistic regression model provided the probability of WZ Sge-type DNe P_{WZ} . We proposed $P_{WZ} = 0.5$ as a classifier which correctly identified 32 in 41 WZ Sge stars and 219 in 225 SU UMa ones. A sample R code to estimate P_{WZ} and the galactic extinctions is provided on our website³. The next *Gaia* data release and further observational studies to increase the statistics will improve our classification method. Our classifier will be a powerful tool to judge a priority target.

Supporting information

The following supplementary information is available in the online article: table E1, E2, and E3.

Acknowledgments

This work was supported by the Grant-in-Aid for JSPS Fellows (No. 17J10039). We are grateful to the survey projects CRTS and ASAS-SN. This work has made use of data from the European Space Agency (ESA) mission *Gaia* (<https://www.cosmos.esa.int/gaia>), processed by the *Gaia* Data Processing and Analysis Consortium (DPAC, <https://www.cosmos.esa.int/web/gaia/dpac/consortium>). Funding for the DPAC has been provided by national institutions, in particular the institutions participating in the *Gaia* Multilateral Agreement. This research has made use of the NASA/IPAC Extragalactic Database (NED), which is operated by the Jet Propulsion Laboratory, California Institute of Technology, under contract with the National Aeronautics and Space Administration. We are also thankful to the AAVSO International Database contributed by many worldwide observers.

References

- Ahn, C. P., et al. 2012, ApJS, 203, 21
- Ak, T., Bilir, S., Ak, S., & Eker, Z. 2008, New Astron., 13, 133
- Bailer-Jones, C. A. L., Rybizki, J., Fouesneau, M., Mantelet, G., & Andrae, R. 2018, AJ, 156, 58
- Bath, G. T. 1973, Nature Physical Science, 246, 84
- Cleveland, W. S. 1979, J. Amer. Statist. Assoc., 74, 829
- Drake, A. J., et al. 2009, ApJ, 696, 870
- Dubus, G., Otolakowska-Hypka, M., & Lasota, J.-P. 2018, ArXiv e-prints
- Evans, D. W., et al. 2018, A&A, 616, A4
- Fernie, J. D. 1989, PASP, 101, 225

- Gaia Collaboration, et al. 2018a, A&A, 616, A10
 Gaia Collaboration, et al. 2018b, A&A, 616, A1
 Gaia Collaboration, et al. 2018c, ArXiv e-prints
 Gaia Collaboration, et al. 2016, A&A, 595, A1
 Hōshi, R. 1979, Progress of Theoret. Phys., 61, 1307
 Hardy, L. K., et al. 2017, MNRAS, 465, 4968
 Hirose, M., & Osaki, Y. 1990, PASJ, 42, 135
 Kato, T. 2015, PASJ, 67, 108
 Kato, T., et al. 2016, PASJ, 68, 65
 Kato, T., et al. 2012a, PASJ, 64, 21
 Kato, T., Maehara, H., & Uemura, M. 2012b, PASJ, 64, 62
 Kato, T., et al. 2010, PASJ, 62, 1525
 Kato, T., Uemura, M., Ishioka, R., Nogami, D., Kunjaya, C.,
 Baba, H., & Yamaoka, H. 2004, PASJ, 56, S1
 Kaur, A., Porter, A., Wilber, A., Wagner, R. M., Woodward,
 C. E., Starrfield, S. G., & Hartmann, D. H. 2014, The
 Astronomer's Telegram, 6624
 Kimura, M., et al. 2016, PASJ, 68, L2
 Knigge, C., Baraffe, I., & Patterson, J. 2011, ApJS, 194, 28
 Kochanek, C. S., et al. 2017, PASP, 129, 104502
 Kolb, U. 1993, A&A, 271, 149
 Kononov, D. A., Bisikalo, D. V., Puzin, V. B., Zhilkin, A. G.,
 & Sytov, A. Y. 2015, Astron. Rep., 59, 191
 Kuulkers, E., Henden, A. A., Honeycutt, R. K., Skidmore, W.,
 Waagen, E. O., & Wynn, G. A. 2011, A&A, 528, A152
 Lin, D. N. C., & Papaloizou, J. 1979, MNRAS, 186, 799
 Lubow, S. H. 1991a, ApJ, 381, 259
 Lubow, S. H. 1991b, ApJ, 381, 268
 Luri, X., et al. 2018, A&A, 616, A9
 Martin, D. C., et al. 2005, ApJ, 619, L1
 Nakata, C., et al. 2013, PASJ, 65, 117
 Neustroev, V. V., et al. 2017, MNRAS, 467, 597
 Osaki, Y. 1974, PASJ, 26, 429
 Osaki, Y. 1989, PASJ, 41, 1005
 Osaki, Y. 1995, PASJ, 47, 47
 Osaki, Y., & Meyer, F. 2002, A&A, 383, 574
 Patterson, J., Augusteijn, T., Harvey, D. A., Skillman, D. R.,
 Abbott, T. M. C., & Thorstensen, J. 1996, PASP, 108, 748
 Pojmański, G. 2002, Acta Astron., 52, 397
 Riello, M., et al. 2018, A&A, 616, A3
 Schlafly, E. F., & Finkbeiner, D. P. 2011, ApJ, 737, 103
 Shappee, B. J., et al. 2014, ApJ, 788, 48
 Skidmore, W., Mason, E., Howell, S. B., Ciardi, D. R., Littlefair,
 S., & Dhillon, V. S. 2000, MNRAS, 318, 429
 Thorstensen, J. R., Alper, E. H., & Weil, K. E. 2016, AJ, 152,
 226
 Verhulst, P.-F. 1845, Nouveaux Mémoires de l'Académie Royale
 des Sciences et Belles-Lettres de Bruxelles, 18, 1
 Verhulst, P.-F. 1847, Nouveaux Mémoires de l'Académie Royale
 des Sciences, des Lettres et des Beaux-Arts de Belgique, 20,
 1
 Wakamatsu, Y., et al. 2017, PASJ, 69, 89
 Warner, B. 1995, Cataclysmic Variable Stars (Cambridge:
 Cambridge University Press)
 Whitehurst, R. 1988, MNRAS, 232, 35

Table 1. Log of observations of ASASSN-14dx

Start *	End *	Mag [†]	σ_{Mag} [‡]	N [§]	Obs
56854.8229	56854.9266	14.253	0.005	38	HaC
56855.8201	56855.9271	14.262	0.005	39	HaC
56856.8167	56856.9272	14.297	0.003	49	HaC
56857.8139	56857.9265	14.282	0.003	50	HaC
56858.8112	56858.9337	14.294	0.003	54	HaC
56859.5509	56859.6768	14.315	0.002	363	MLF
56859.8084	56859.9330	14.307	0.004	55	HaC
56860.8056	56860.9328	14.304	0.004	56	HaC
56861.8034	56861.8096	14.373	0.020	4	HaC
56862.8009	56862.9326	14.355	0.003	58	HaC
56863.7981	56863.9319	14.360	0.003	59	HaC
56864.7953	56864.9323	14.379	0.003	49	HaC
56865.7925	56865.9323	14.403	0.003	50	HaC
56866.7897	56866.9305	14.404	0.004	51	HaC
56867.7870	56867.9299	14.405	0.004	51	HaC
56868.7844	56868.9290	14.415	0.003	53	HaC
56869.7814	56869.9299	14.377	0.004	53	HaC
56870.7787	56870.9299	14.417	0.003	54	HaC
56871.7759	56871.9301	14.413	0.004	55	HaC
56872.7731	56872.9294	14.424	0.005	56	HaC
56873.7703	56873.9290	14.468	0.004	57	HaC
56874.7675	56874.9293	14.451	0.004	58	HaC
56875.7648	56875.9271	14.501	0.003	58	HaC
56876.7620	56876.9269	14.483	0.003	59	HaC
56879.7537	56879.9099	14.514	0.005	56	HaC
56880.7509	56880.9092	14.505	0.005	57	HaC
56881.7473	56881.9103	14.516	0.003	78	HaC
56882.7454	56882.9090	14.520	0.003	78	HaC
56885.7655	56885.9145	14.479	0.005	49	HaC
56886.7627	56886.9115	14.509	0.004	56	HaC
56887.7599	56887.9091	14.511	0.004	49	HaC
56888.7572	56888.9092	14.512	0.004	50	HaC
56889.7544	56889.8950	14.516	0.004	45	HaC
56890.7516	56890.9099	14.535	0.003	52	HaC
56891.7488	56891.9070	14.552	0.003	52	HaC
56892.7461	56892.8787	14.547	0.004	43	HaC
56893.7433	56893.8719	14.548	0.004	42	HaC
56894.7412	56894.8815	14.555	0.005	46	HaC
56895.7384	56895.9052	14.565	0.004	55	HaC
56896.7357	56896.9058	14.561	0.004	56	HaC
56897.7329	56897.9055	14.584	0.004	57	HaC
56898.7121	56898.9034	14.554	0.004	64	HaC
56900.7245	56900.9039	14.548	0.004	59	HaC
56901.7217	56901.9030	14.587	0.003	60	HaC

*BJD−2400000.

†Mean magnitude. All observations are no filter (clear).

‡Standard deviation of the observed magnitude.

§Number of observations.

||Observer's code: HaC(F. J. Hambach), MLF (B. Monard), KU1 (Kyoto U. team), Kis (S. Kiyota)

Table 1. Log of observations of ASASSN-14dx (continued)

Start *	End *	Mag [†]	σ_{Mag} [‡]	N [§]	Obs
56902.7190	56902.9003	14.592	0.004	60	HaC
56903.7495	56903.8999	14.575	0.005	50	HaC
56904.7230	56904.7815	14.575	0.007	20	HaC
56905.7456	56905.8983	14.576	0.004	51	HaC
56906.7442	56906.8995	14.606	0.004	52	HaC
56907.8263	56907.9158	14.626	0.006	37	HaC
56908.7389	56908.8979	14.630	0.005	54	HaC
56909.7361	56909.8972	14.648	0.005	55	HaC
56911.7306	56911.8933	14.627	0.005	54	HaC
56913.7249	56913.8583	14.610	0.009	38	HaC
56914.7228	56914.8909	14.623	0.004	60	HaC
56915.7200	56915.8900	14.595	0.003	61	HaC
56916.7173	56916.8892	14.620	0.004	62	HaC
56919.7089	56919.8871	14.646	0.004	65	HaC
56920.7061	56920.8864	14.638	0.004	66	HaC
56921.7033	56921.8856	14.631	0.004	67	HaC
56922.7006	56922.8849	14.639	0.003	68	HaC
56923.6978	56923.8844	14.626	0.006	68	HaC
56924.6951	56924.8836	14.647	0.004	70	HaC
56925.6923	56925.8821	14.646	0.005	69	HaC
56926.6895	56926.8821	14.632	0.005	72	HaC
56927.6867	56927.8818	14.667	0.004	74	HaC
56928.6839	56928.8772	14.655	0.004	72	HaC
56929.6811	56929.8764	14.665	0.004	74	HaC
56930.6783	56930.8735	14.678	0.006	74	HaC
56931.6756	56931.8789	14.696	0.004	78	HaC
56934.8403	56934.8701	14.648	0.005	16	HaC
56935.6652	56935.8720	14.702	0.003	79	HaC
56936.6624	56936.8713	14.720	0.004	80	HaC
56937.6596	56937.8701	14.717	0.004	81	HaC
56938.6569	56938.8699	14.751	0.006	89	HaC
56939.6540	56939.8703	14.706	0.005	87	HaC
56940.6680	56940.8624	14.699	0.008	79	HaC
56941.6652	56941.8679	14.723	0.005	71	HaC
56942.7241	56942.8669	14.724	0.006	51	HaC
56943.6597	56943.8652	14.730	0.005	72	HaC
56944.6569	56944.8654	14.751	0.004	73	HaC
56945.6569	56945.8659	14.748	0.004	72	HaC
56946.6513	56946.8628	14.760	0.004	73	HaC
56947.6492	56947.8599	14.768	0.006	74	HaC
56948.6464	56948.8607	14.780	0.004	75	HaC
56949.6436	56949.8581	14.785	0.005	75	HaC
56950.6408	56950.8524	14.750	0.003	74	HaC
56951.6380	56951.8478	14.798	0.005	69	HaC
56953.6321	56953.8505	14.865	0.004	76	HaC
56954.6856	56954.8491	14.882	0.006	57	HaC
56955.6828	56955.8494	14.854	0.005	58	HaC
56957.3066	56957.3752	14.864	0.002	198	MLF
56959.6718	56959.8469	14.889	0.006	65	HaC
56960.6689	56960.8466	14.893	0.005	66	HaC

Table 1. Log of observations of ASASSN-14dx (continued)

Start *	End *	Mag [†]	σ_{Mag} [‡]	N [§]	Obs
56961.6662	56961.8438	14.888	0.005	66	HaC
56962.6634	56962.8444	14.887	0.005	72	HaC
56963.6607	56963.8436	14.899	0.006	73	HaC
56964.6579	56964.8429	14.870	0.004	74	HaC
56965.7484	56965.8428	14.864	0.006	44	HaC
56966.6530	56966.8416	14.886	0.005	76	HaC
56967.6647	56967.8408	14.915	0.008	76	HaC
56968.6625	56968.8422	14.876	0.007	77	HaC
56969.6597	56969.8317	14.846	0.008	79	HaC
56970.5876	56970.8292	14.808	0.004	96	HaC
56971.6603	56971.8280	14.846	0.005	62	HaC
56972.6540	56972.8281	14.830	0.004	65	HaC
56973.6512	56973.8279	14.823	0.004	66	HaC
56974.6484	56974.8278	14.848	0.004	67	HaC
56975.6457	56975.8278	14.849	0.004	68	HaC
56976.6429	56976.8278	14.921	0.005	69	HaC
56977.6401	56977.8251	14.934	0.004	69	HaC
56979.6346	56979.8246	14.944	0.004	71	HaC
56980.6619	56980.8250	14.929	0.003	60	HaC
56981.6591	56981.8250	14.941	0.004	62	HaC
56982.6563	56982.8249	14.924	0.004	63	HaC
56983.6535	56983.8247	14.951	0.004	64	HaC
56984.6507	56984.7856	14.941	0.003	54	HaC
56985.6528	56985.7813	14.925	0.004	46	HaC
56986.6907	56986.7788	14.920	0.004	31	HaC
56987.6492	56987.7766	14.940	0.004	45	HaC
56988.5774	56988.6999	14.899	0.002	316	KU1
56988.6464	56988.7732	14.930	0.003	45	HaC
56989.6436	56989.7702	14.913	0.004	45	HaC
56990.6408	56990.7677	14.925	0.004	45	HaC
56991.6381	56991.7655	14.930	0.005	45	HaC
56992.6353	56992.7627	14.932	0.003	45	HaC
56993.6325	56993.7600	14.951	0.006	45	HaC
56994.6297	56994.7580	14.928	0.007	56	HaC
56995.6442	56995.7552	14.946	0.007	48	HaC
56997.6423	56997.7504	14.952	0.011	41	HaC
56998.6403	56998.7476	14.933	0.008	41	HaC
56999.6374	56999.7449	14.935	0.005	41	HaC
57000.6346	57000.7399	14.981	0.008	40	HaC
57002.6844	57002.7344	14.945	0.007	21	HaC
57003.6817	57003.7316	14.937	0.007	21	HaC
57004.6789	57004.7290	14.961	0.008	21	HaC
57005.6762	57005.7262	14.914	0.014	21	HaC
57007.6331	57007.7219	14.935	0.004	53	HaC
57008.6678	57008.7187	14.905	0.008	24	HaC
57013.8881	57014.0847	14.950	0.003	520	Kis
57317.0156	57317.0932	15.347	0.007	196	KU1
57317.9675	57318.1806	15.332	0.003	561	KU1

Table 2. List of WZ Sge-type DNe and candidates identified with *Gaia* DR2 objects

Name	Plx*	G^{\dagger}	$G_{\text{col}}^{\ddagger}$	A_G^{\S}	$A_{\text{BP}} - A_{\text{RP}}^{\S}$	$P_{\text{orb}}^{\parallel}$	$P_{\text{WZ}}^{\dagger\dagger}$
SDSS J160501.35+203056.9	3.11(55)	19.822(6)	0.066(87)	0.179(14)	0.100(18)	0.05666	0.97(2)
OT J012059.59 +325545.0	2.80(50)	19.852(6)	0.018(124)	0.118(13)	0.066(17)	0.05716	0.97(3)
EG Cnc	5.44(31)	18.812(2)	0.175(35)	0.085(4)	0.048(6)	0.05997	0.96(1)
QZ Lib	5.34(33)	18.880(10)	0.262(62)	0.222(13)	0.124(17)	0.06413	0.95(3)
DY CMi	3.29(42)	19.505(3)	0.099(52)	0.043(6)	0.024(8)	0.05937 [#]	0.94(3)
CRTS J224739.7-362254	3.22(52)	19.649(5)	0.131(67)	0.033(2)	0.019(2)	0.05572 [#]	0.94(5)
TCP J18154219+3515598	4.57(25)	19.193(4)	0.240(69)	0.065(4)	0.037(5)	0.06022 [#]	0.94(3)
PQ And	3.98(45)	19.063(5)	0.126(69)	0.085(11)	0.047(14)	0.05600	0.93(4)
1RXS J023238.8-371812	4.83(20)	18.675(6)	0.150(46)	0.068(2)	0.038(2)	0.06500	0.93(2)
EZ Lyn	6.87(15)	17.810(2)	0.128(19)	0.078(2)	0.044(3)	0.05900	0.92(1)
UZ Boo	3.62(61)	19.992(6)	0.383(77)	0.068(4)	0.038(6)	0.06051 [#]	0.91(7)
WZ Sge	22.16(4)	15.210(3)	0.153(19)	0.048(0)	0.027(0)	0.05669	0.90(1)
V624 Peg	4.64(31)	18.424(5)	0.159(31)	0.177(12)	0.098(17)	0.05865	0.88(4)
PNV J03093063+2638031	4.09(28)	18.652(15)	0.214(79)	0.339(21)	0.189(28)	0.05615	0.86(7)
V355 UMa	6.66(9)	17.383(2)	0.082(15)	0.018(0)	0.010(0)	0.05729	0.85(1)
SSS J122221.7-311523	4.26(36)	18.851(12)	0.266(75)	0.119(9)	0.066(12)	0.07588	0.84(8)
SDSS J161027.61+090738.4	2.63(51)	19.838(16)	0.250(125)	0.096(7)	0.053(10)	0.05687	0.83(16)
ASASSN-14cv	3.43(21)	19.004(16)	0.179(102)	0.071(3)	0.040(4)	0.05992	0.82(11)
V406 Vir	5.91(16)	17.718(7)	0.152(35)	0.061(1)	0.034(2)	0.05592	0.82(4)
ASASSN-14jv	3.52(18)	18.697(18)	0.141(95)	0.164(9)	0.091(12)	0.05442	0.81(10)
V1838 Aql	4.95(17)	17.866(9)	0.188(47)	0.362(20)	0.202(26)	0.05706	0.79(6)
ASAS J102522-1542.4	3.91(52)	19.357(15)	0.438(86)	0.160(16)	0.090(22)	0.06136	0.76(15)
BW Scl	10.60(10)	16.262(4)	0.164(26)	0.019(0)	0.011(0)	0.05432	0.72(4)
GW Lib	8.87(8)	16.490(7)	0.166(28)	0.175(2)	0.098(3)	0.05332	0.72(4)
FL Psc	6.51(14)	17.527(6)	0.279(27)	0.165(3)	0.092(4)	0.05610	0.70(4)
OV Boo	4.74(14)	18.234(6)	0.259(49)	0.038(1)	0.021(1)	0.04626	0.69(8)
PNV J17144255-2943481	5.64(15)	17.163(7)	0.151(52)	0.249(10)	0.139(13)	0.05956	0.64(9)
ASASSN-17el	2.91(17)	18.680(4)	0.131(43)	0.071(3)	0.040(4)	0.05516	0.63(9)
HV Vir	2.90(41)	19.138(9)	0.276(61)	0.083(3)	0.046(4)	0.05707	0.61(17)
PNV J23052314-0225455	2.78(42)	19.047(25)	0.249(122)	0.152(7)	0.085(9)	0.05456	0.60(25)
EQ Lyn	2.70(39)	18.968(6)	0.276(37)	0.129(11)	0.072(16)	0.05278	0.48(16)
V455 And	13.24(6)	16.064(4)	0.419(21)	0.064(1)	0.036(1)	0.05631	0.47(4)
ASASSN-14cl	3.83(19)	18.187(13)	0.400(53)	0.091(5)	0.051(6)	0.05838	0.26(8)
SDSS J145758.21+514807.9	1.72(31)	19.821(13)	0.435(111)	0.067(2)	0.038(1)	0.05409	0.18(16)
MASTER OT J085854.16-274030.7	2.03(35)	19.092(6)	0.381(55)	0.219(36)	0.123(49)	0.05475 [#]	0.17(12)
BC UMa	3.12(18)	18.370(4)	0.427(29)	0.056(1)	0.031(1)	0.06261	0.14(4)
V627 Peg	10.03(7)	15.667(4)	0.380(37)	0.050(1)	0.028(1)	0.05452	0.14(3)
ASASSN-16eg	2.25(32)	19.506(8)	0.694(67)	0.049(3)	0.027(4)	0.07548	0.06(4)
RZ Leo	3.56(25)	18.241(12)	0.791(50)	0.058(2)	0.032(2)	0.07604	0.02(1)
WZ Sge-type DN candidates.							
SSS J200331.3-284938	3.10(47)	19.564(18)	0.380(107)	0.195(21)	0.109(29)	0.05871	0.74(19)
PNV J19321040-2052505	3.00(50)	19.141(8)	0.298(46)	0.130(20)	0.073(28)	—	0.63(18)
ASASSN-17kg	3.31(51)	19.147(8)	0.366(41)	0.109(7)	0.061(9)	0.05660 [#]	0.62(17)
ASASSN-14dx	12.34(4)	14.959(25)	0.232(127)	0.034(1)	0.019(1)	0.05751	0.21(14)
ASASSN-14dx in quiescence**	12.34(4)	16.254(42)	-0.112(74)	0.037(0)	0.020(0)	0.05751	0.97(1)

*Parallax ϖ obtained by *Gaia* DR2 in units of mas.†*Gaia G* magnitude‡*Gaia* color $G_{\text{col}} = G_{\text{BP}} - G_{\text{RP}}$ in units of magnitude§Galactic extinction in G , G_{BP} and G_{RP} in units of magnitude. The estimation method is described in section 4.2.

||Orbital period in units of day

††WZ Sge-type DN probability P_{WZ} . $P_{\text{WZ}} = 0.5$ is a borderline between WZ Sge/SU UMa stars.Objects with $P_{\text{WZ}} > 0.5$ are good candidates of WZ Sge stars.** G and G_{col} in quiescence are calculated by using the SDSS DR9.

#Orbital periods estimated from superhump ones by using equation (6) in Kato et al. (2012a).

Table 3. List of SU UMa-type DNe identified with *Gaia* DR2 objects

Name	Plx*	G^{\dagger}	$G_{\text{col}}^{\ddagger}$	A_G^{\S}	$A_{\text{BP}} - A_{\text{RP}}^{\S}$	$P_{\text{orb}}^{\parallel}$	$P_{\text{WZ}}^{\dagger\dagger}$
MASTER OT J220559.40-341434.9	6.23(27)	18.344(5)	0.157(30)	0.045(2)	0.025(2)	0.06128	0.95(1)
MASTER OT J143857.37+703523.1	3.82(26)	19.371(4)	0.146(49)	0.035(2)	0.019(2)	—	0.94(2)
ASASSN-15lt	2.50(48)	19.696(23)	0.193(186)	0.192(20)	0.107(26)	—	0.84(20)
SDSS J150137.22+550123.4	2.93(28)	19.257(5)	0.144(56)	0.030(1)	0.017(1)	0.05684	0.82(8)
XZ Eri	3.00(30)	19.247(9)	0.275(96)	0.075(4)	0.042(5)	0.06116	0.69(16)
ASASSN-17eq	2.81(38)	19.956(25)	0.519(149)	0.059(4)	0.033(5)	—	0.55(28)
ASASSN-15ev	2.26(38)	19.574(16)	0.423(83)	0.410(38)	0.231(52)	—	0.47(24)
ASASSN-15fo	2.44(41)	19.474(11)	0.470(101)	0.157(24)	0.088(33)	—	0.31(21)
MM Hya	2.77(23)	18.701(17)	0.324(88)	0.105(6)	0.059(8)	0.05759	0.30(15)
GP CVn	2.75(20)	18.791(12)	0.344(74)	0.039(1)	0.022(1)	0.06295	0.27(12)
DT Pyx	2.88(29)	19.012(8)	0.482(49)	0.201(21)	0.113(30)	0.06165	0.27(11)
NZ Boo	5.36(9)	17.342(10)	0.363(54)	0.030(0)	0.017(0)	0.05891	0.24(7)
SDSS J090350.73+330036.1	2.52(38)	19.064(17)	0.422(87)	0.055(3)	0.031(4)	0.05907	0.21(14)
TV Crv	3.07(30)	18.679(7)	0.467(43)	0.163(7)	0.092(10)	0.06288	0.21(8)
ASASSN-14hl	1.21(23)	19.929(14)	0.219(118)	0.035(1)	0.020(0)	—	0.20(18)
WX Cet	3.79(16)	18.137(7)	0.427(40)	0.044(1)	0.025(1)	0.05826	0.19(5)
VY Aqr	7.24(14)	16.865(27)	0.519(116)	0.181(5)	0.102(6)	0.06309	0.17(11)
ASASSN-17kc	1.95(35)	19.196(10)	0.367(72)	0.127(5)	0.071(6)	—	0.17(12)
MASTER OT J003831.10-640313.7	3.00(16)	18.312(11)	0.369(61)	0.040(1)	0.022(1)	—	0.15(6)
ASASSN-17qn	2.49(44)	19.819(14)	0.731(120)	0.192(23)	0.108(33)	—	0.15(14)
CRTS J215815.3+094709	3.70(16)	17.488(19)	0.291(94)	0.113(4)	0.063(5)	—	0.15(8)
OY Car	11.01(3)	15.620(34)	0.427(145)	0.077(2)	0.043(1)	0.06312	0.15(12)
UV Per	3.99(13)	17.926(8)	0.488(48)	0.169(9)	0.095(12)	0.06489	0.14(4)
FZ Cet	2.89(17)	18.244(26)	0.347(128)	0.030(1)	0.017(1)	—	0.14(10)
ASASSN-17fo	2.51(43)	19.158(16)	0.528(97)	0.051(2)	0.029(2)	0.06155	0.13(11)
ASASSN-15sp	1.84(35)	19.789(20)	0.660(131)	0.493(72)	0.279(102)	—	0.12(14)
QZ Vir	7.81(7)	16.055(12)	0.363(50)	0.036(0)	0.020(0)	0.05882	0.12(4)
V359 Cen	2.69(23)	18.753(12)	0.539(67)	0.261(18)	0.147(26)	0.07790	0.12(6)
CC Scl	4.90(15)	16.882(10)	0.323(48)	0.032(1)	0.018(1)	0.05857	0.11(3)
ASASSN-15mb	2.45(21)	19.066(15)	0.525(85)	0.043(1)	0.024(1)	—	0.11(6)
SW UMa	6.15(8)	16.576(10)	0.391(40)	0.058(1)	0.033(1)	0.05682	0.10(3)
CRTS J034515.4-015216	2.61(37)	18.930(16)	0.606(114)	0.313(17)	0.176(23)	0.07018	0.10(9)
MASTER OT J004527.52+503213.8	3.29(32)	18.974(7)	0.755(58)	0.227(26)	0.128(37)	0.07800	0.09(5)
MASTER OT J072948.66+593824.4	2.70(51)	19.000(23)	0.605(86)	0.104(12)	0.058(17)	—	0.09(8)
ASASSN-18gn	2.26(43)	19.764(12)	0.755(95)	0.228(43)	0.129(61)	—	0.09(9)
IY UMa	5.60(10)	17.438(23)	0.596(84)	0.019(0)	0.010(0)	0.07391	0.09(5)
2QZ J015940.6-281040	2.58(37)	19.157(9)	0.609(105)	0.029(1)	0.016(1)	—	0.09(7)
BC Dor	2.63(16)	18.813(9)	0.566(64)	0.157(5)	0.088(7)	0.06613	0.08(4)
SDSS J140037.99+572341.3	1.81(26)	18.878(18)	0.327(96)	0.034(1)	0.019(1)	0.06300	0.08(7)
NSV 4618	5.47(12)	16.851(18)	0.442(69)	0.070(2)	0.039(2)	0.06577	0.08(3)
ASASSN-17gf	2.07(17)	18.517(12)	0.409(74)	0.396(41)	0.222(56)	—	0.08(5)
V521 Peg	5.23(9)	17.044(7)	0.495(38)	0.083(1)	0.047(2)	0.05990	0.07(2)
CRTS J044027.1+023301	2.31(26)	18.673(19)	0.550(92)	0.414(25)	0.234(34)	—	0.07(5)
GO Com	2.64(24)	18.324(13)	0.438(67)	0.022(0)	0.012(0)	0.06580	0.06(3)
CRTS J164950.4+035835	2.33(26)	18.649(10)	0.504(44)	0.200(11)	0.112(15)	—	0.06(3)

*Parallax ϖ obtained by *Gaia* DR2 in units of mas.†*Gaia G* magnitude‡*Gaia* color $G_{\text{col}} = G_{\text{BP}} - G_{\text{RP}}$ in units of magnitude§Galactic extinction in G , G_{BP} and G_{RP} in units of magnitude. The estimation method is described in section 4.2.

||Orbital period in units of day

††WZ Sge-type DN probability P_{WZ} . $P_{\text{WZ}} = 0.5$ is a borderline between WZ Sge/SU UMa stars.Objects with $P_{\text{WZ}} > 0.5$ are good candidates of WZ Sge stars.

Table 3. List of SU UMa-type DNe identified with *Gaia* DR2 objects (continued)

Name	Plx*	G^{\dagger}	$G_{\text{col}}^{\ddagger}$	A_G^{\S}	$A_{\text{BP}} - A_{\text{RP}}^{\S}$	$P_{\text{orb}}^{\parallel}$	$P_{\text{WZ}}^{\dagger\dagger}$
ASASSN-14kb	2.91(19)	18.667(32)	0.638(187)	0.155(7)	0.087(8)	0.06811	0.06(7)
V436 Cen	6.36(6)	16.323(30)	0.446(136)	0.114(3)	0.064(3)	0.06250	0.06(5)
PNV J06501960+3002449	2.64(24)	18.443(32)	0.514(174)	0.137(14)	0.077(19)	—	0.06(7)
SDSS J182142.83+212153.5	2.03(29)	19.272(10)	0.628(58)	0.274(30)	0.155(43)	—	0.06(4)
ASASSN-14je	1.70(32)	19.563(26)	0.598(136)	0.222(16)	0.125(22)	0.06700	0.05(6)
V844 Her	3.41(10)	17.489(16)	0.396(62)	0.020(0)	0.011(0)	0.05464	0.05(2)
OV Dra	2.14(15)	18.592(25)	0.480(88)	0.043(1)	0.024(1)	0.05874	0.04(2)
SDSS J033449.86-071047.8	2.33(30)	18.746(13)	0.605(65)	0.112(4)	0.063(5)	0.07900	0.03(2)
BZ UMa	6.56(6)	16.206(17)	0.511(63)	0.077(1)	0.043(1)	0.06799	0.03(1)
VW Hyi	18.53(2)	13.837(19)	0.484(85)	0.077(1)	0.044(1)	0.07427	0.03(2)
MASTER OT J120251.56-454116.7	2.22(24)	18.990(19)	0.670(95)	0.177(16)	0.100(22)	—	0.03(2)
SY Cap	2.60(18)	18.104(10)	0.518(44)	0.152(6)	0.086(9)	—	0.03(1)
OGLE-BLG-DN-0254	3.76(16)	18.092(16)	0.761(61)	0.213(14)	0.120(20)	0.07193	0.03(1)
V630 Cyg	2.22(32)	19.193(15)	0.808(93)	0.404(68)	0.229(99)	—	0.03(3)
AY For	2.09(24)	18.304(18)	0.418(82)	0.039(1)	0.022(1)	0.07460	0.03(2)
SDSS J131432.10+444138.7	1.48(25)	19.089(15)	0.431(92)	0.045(1)	0.025(1)	—	0.03(2)
ASASSN-17hm	2.30(43)	19.961(19)	1.058(130)	0.406(105)	0.230(156)	—	0.03(4)
V1024 Per	3.98(7)	17.062(21)	0.554(94)	0.329(10)	0.186(12)	0.07060	0.03(2)
V493 Ser	3.24(21)	18.327(9)	0.783(57)	0.309(12)	0.174(16)	0.07408	0.03(1)
EG Aqr	2.96(38)	18.971(24)	0.855(163)	0.074(3)	0.042(4)	0.07596	0.02(3)
ASASSN-15au	2.36(18)	17.877(12)	0.395(75)	0.046(3)	0.026(4)	—	0.02(1)
MASTER OT J064725.70+491543.9	3.73(15)	17.372(20)	0.561(95)	0.139(6)	0.078(8)	0.06554	0.02(2)
SDSS J032015.29+441059.3	2.11(24)	18.870(30)	0.676(185)	0.273(33)	0.154(46)	0.06870	0.02(3)
HT Cas	7.07(6)	16.351(11)	0.668(48)	0.115(2)	0.065(2)	0.07365	0.02(1)
CRTS J170609.7+143452	2.26(18)	18.123(22)	0.526(92)	0.309(12)	0.174(16)	0.05823	0.02(2)
ASASSN-14ag	5.63(9)	16.180(23)	0.465(109)	0.043(1)	0.024(1)	0.06031	0.02(2)
BB Ari	2.83(19)	18.450(12)	0.744(65)	0.231(10)	0.130(14)	0.07020	0.02(1)
CRTS J050659.2-165932	1.78(23)	18.663(14)	0.499(81)	0.155(6)	0.087(8)	—	0.02(2)
AQ CMi	1.55(27)	18.675(26)	0.434(135)	0.159(27)	0.089(37)	0.06490	0.02(2)
CRTS J094327.3-272039	2.07(27)	18.611(28)	0.618(135)	0.232(21)	0.131(29)	—	0.02(2)
MR UMa	2.93(17)	17.893(7)	0.580(44)	0.052(1)	0.029(1)	0.06337	0.02(1)
CU Vel	6.29(6)	16.712(13)	0.772(57)	0.254(5)	0.143(6)	0.07850	0.02(1)
V1028 Cyg	1.73(22)	18.890(21)	0.611(152)	0.307(31)	0.173(43)	—	0.02(2)
V2051 Oph	8.90(7)	15.367(9)	0.590(45)	0.186(3)	0.105(3)	0.06243	0.02(1)
ASASSN-13cz	1.75(22)	18.775(9)	0.514(41)	0.041(1)	0.023(1)	0.07700	0.02(1)
SDSS J110014.72+131552.1	2.17(29)	18.681(42)	0.623(196)	0.040(2)	0.022(1)	0.06560	0.02(2)
ASASSN-13cx	2.26(23)	18.054(22)	0.526(100)	0.210(16)	0.118(22)	0.07965	0.02(1)
EF Peg	3.92(45)	18.080(11)	0.853(46)	0.108(12)	0.061(17)	0.08370	0.02(1)
CRTS J163120.9+103134	2.03(12)	18.522(14)	0.594(109)	0.192(5)	0.108(5)	0.06265	0.02(1)
AY Lyr	2.22(13)	17.932(34)	0.464(153)	0.121(7)	0.068(8)	0.07330	0.02(2)
1RXS J185310.0+594509	1.53(15)	18.489(12)	0.396(70)	0.102(4)	0.057(5)	0.05826	0.01(1)
ASASSN-13bj	1.80(21)	18.523(26)	0.503(121)	0.067(2)	0.038(2)	—	0.01(1)
V776 And	2.45(15)	18.119(11)	0.628(54)	0.249(11)	0.141(15)	0.06400	0.01(1)
TY Psc	3.83(10)	16.866(26)	0.516(113)	0.115(3)	0.065(4)	0.06833	0.01(1)
SDSS J152419.33+220920.0	2.15(29)	19.143(30)	0.810(131)	0.119(4)	0.067(4)	0.06532	0.01(1)
Mis V1446	2.01(26)	18.906(25)	0.714(149)	0.172(28)	0.097(39)	—	0.01(2)
MASTER OT J162323.48+782603.3	2.51(16)	18.448(14)	0.695(66)	0.079(2)	0.044(3)	—	0.01(1)
QW Ser	2.65(26)	17.580(17)	0.487(66)	0.081(3)	0.046(3)	0.07453	0.01(1)
V650 Peg	2.52(34)	18.735(14)	0.827(114)	0.222(11)	0.125(14)	—	0.01(1)
V485 Cen	3.10(30)	17.813(38)	0.672(192)	0.155(11)	0.088(14)	0.04100	0.01(2)
CT Hya	1.40(26)	18.547(27)	0.378(115)	0.082(4)	0.046(4)	0.06520	0.01(1)

Table 3. List of SU UMa-type DNe identified with *Gaia* DR2 objects (continued)

Name	Plx*	G^{\dagger}	$G_{\text{col}}^{\ddagger}$	A_G^{\S}	$A_{\text{BP}} - A_{\text{RP}}^{\S}$	$P_{\text{orb}}^{\parallel}$	$P_{\text{WZ}}^{\parallel\parallel}$
ASASSN-13bm	2.30(20)	18.775(20)	0.783(94)	0.191(11)	0.107(16)	—	0.01(1)
ASASSN-18fp	2.09(28)	18.288(20)	0.608(146)	0.279(18)	0.157(24)	—	0.01(1)
SDSS J091001.63+164820.0	1.87(28)	18.750(17)	0.618(68)	0.081(3)	0.046(4)	—	0.01(1)
DH Aql	3.55(19)	17.966(9)	0.852(66)	0.250(17)	0.141(24)	—	0.01(1)
HO Del	1.98(22)	18.211(28)	0.547(135)	0.153(14)	0.086(19)	0.06266	0.01(1)
GZ Cet	3.57(23)	18.365(14)	0.937(109)	0.074(2)	0.042(3)	0.05534	0.01(1)
AX For	2.97(18)	17.798(15)	0.658(80)	0.049(1)	0.028(1)	0.07850	0.01(1)
V391 Cam	6.09(5)	15.532(11)	0.500(49)	0.185(2)	0.104(3)	0.05620	0.01(0)
CY UMa	3.18(14)	17.305(26)	0.567(136)	0.031(1)	0.017(1)	0.06795	0.01(1)
ASASSN-14ex	1.42(28)	19.090(22)	0.617(123)	0.104(10)	0.059(13)	—	0.01(1)
SDSS J162520.29+120308.7	2.20(24)	18.451(12)	0.732(64)	0.196(7)	0.111(9)	0.09111	0.01(0)
V4140 Sgr	1.67(16)	17.719(9)	0.346(59)	0.174(5)	0.098(7)	0.06143	0.01(0)
DV UMa	2.60(35)	18.673(19)	0.865(96)	0.017(1)	0.010(1)	0.08585	0.01(1)
CRTS J202731.2-224002	2.95(16)	17.890(10)	0.749(51)	0.127(5)	0.072(6)	0.07000	0.01(0)
V1258 Cen	2.81(39)	18.829(43)	1.004(163)	0.160(13)	0.090(18)	0.08894	0.01(1)
TU Crt	3.22(14)	17.754(13)	0.772(55)	0.101(3)	0.057(4)	0.08209	0.01(0)
NSV 4838	1.57(30)	18.553(19)	0.538(99)	0.036(1)	0.020(1)	0.06790	0.01(1)
TY PsA	5.43(7)	15.795(27)	0.524(91)	0.038(1)	0.021(1)	0.08410	0.01(0)
AQ Eri	2.66(12)	17.211(14)	0.522(71)	0.149(5)	0.084(6)	0.06094	0.01(0)
V893 Sco	8.06(5)	14.647(17)	0.516(73)	0.262(4)	0.148(4)	0.07596	0.01(0)
V342 Cam	3.52(11)	17.647(14)	0.850(65)	0.216(7)	0.122(10)	0.07531	0.01(0)
AR Pic	3.14(8)	17.147(12)	0.606(57)	0.109(2)	0.061(3)	0.08022	0.01(0)
ASASSN-17ex	1.54(23)	18.902(13)	0.736(77)	0.351(47)	0.198(68)	—	0.01(0)
SDSS J100515.38+191107.9	2.57(24)	18.050(15)	0.728(131)	0.063(2)	0.036(2)	0.07472	0.01(1)
SU UMa	4.53(3)	15.292(47)	0.312(129)	0.083(2)	0.046(1)	0.07638	0.00(0)
SX LMi	3.08(12)	16.693(42)	0.471(160)	0.071(2)	0.040(2)	0.06717	0.00(1)
MASTER OT J042609.34+354144.8	5.32(7)	16.209(17)	0.743(69)	0.323(7)	0.182(9)	0.06560	0.00(0)
AW Gem	2.13(29)	19.081(13)	0.945(85)	0.143(14)	0.080(20)	0.07621	0.00(0)
SDSS J114628.80+675909.7	1.45(16)	18.203(11)	0.434(48)	0.031(0)	0.017(0)	—	0.00(0)
KV Dra	2.22(6)	17.254(18)	0.440(75)	0.033(1)	0.018(0)	0.05876	0.00(0)
FO And	1.67(16)	17.975(51)	0.499(268)	0.131(8)	0.074(8)	0.07161	0.00(1)
ASASSN-14dw	1.80(32)	18.198(9)	0.626(56)	0.191(21)	0.107(30)	—	0.00(0)
LY Hya	3.14(16)	17.994(66)	0.900(296)	0.106(7)	0.060(6)	0.07480	0.00(1)
AK Cnc	1.69(19)	18.236(10)	0.577(73)	0.076(2)	0.043(3)	0.06510	0.00(0)
RX J1715.6+6856	1.38(15)	18.357(19)	0.494(81)	0.082(2)	0.046(2)	0.06830	0.00(0)
CTCV J1940-4724	2.86(6)	16.732(56)	0.489(233)	0.112(5)	0.063(4)	0.08090	0.00(1)
CRTS J105122.8+672528	0.99(19)	18.647(22)	0.373(101)	0.034(1)	0.019(0)	0.05960	0.00(0)
PU CMa	6.13(3)	15.245(18)	0.547(74)	0.076(1)	0.043(1)	0.05669	0.00(0)
DM Lyr	1.53(12)	18.427(24)	0.654(137)	0.289(19)	0.163(25)	0.06541	0.00(0)
CRTS J102842.9-081927	1.45(29)	19.359(14)	0.845(300)	0.129(7)	0.073(6)	0.03620	0.00(1)
TT Boo	1.47(20)	18.955(18)	0.714(77)	0.035(1)	0.019(0)	0.07594	0.00(0)
ASASSN-16my	1.61(19)	18.624(12)	0.781(72)	0.412(64)	0.233(92)	—	0.00(0)
ASASSN-17dg	2.58(18)	18.151(16)	0.899(71)	0.259(25)	0.146(36)	—	0.00(0)
CRTS J081418.9-005022	1.87(20)	18.334(20)	0.705(100)	0.078(6)	0.044(8)	0.07485	0.00(0)
SSS J134850.1-310835	2.79(26)	18.268(25)	0.949(127)	0.111(7)	0.063(9)	—	0.00(0)
1RXS J003828.7+250920	2.10(33)	18.786(25)	0.914(122)	0.071(3)	0.040(5)	—	0.00(0)
1RXS J161659.5+620014	2.03(8)	17.559(36)	0.541(160)	0.037(1)	0.021(1)	—	0.00(0)
WY Tri	2.04(13)	17.633(24)	0.611(101)	0.177(6)	0.099(8)	0.07569	0.00(0)
CRTS J033349.8-282244	1.63(22)	18.081(13)	0.560(55)	0.022(0)	0.012(0)	—	0.00(0)
OT J055717+683226	1.48(16)	18.285(7)	0.618(33)	0.206(9)	0.116(13)	0.05230	0.00(0)
V1040 Cen	7.80(3)	14.035(17)	0.421(73)	0.118(2)	0.066(1)	0.06049	0.00(0)
SDSS J164248.52+134751.4	1.85(12)	17.826(12)	0.626(55)	0.164(3)	0.092(4)	0.07710	0.00(0)
SDSS J083845.23+491055.5	1.30(23)	18.329(23)	0.545(99)	0.096(2)	0.054(2)	0.06920	0.00(0)
ASASSN-13ak	1.35(25)	19.042(17)	0.773(96)	0.093(3)	0.052(4)	—	0.00(0)

Table 3. List of SU UMa-type DNe identified with *Gaia* DR2 objects (continued)

Name	Plx*	G^{\dagger}	$G_{\text{col}}^{\ddagger}$	A_G^{\S}	$A_{\text{BP}} - A_{\text{RP}}^{\S}$	$P_{\text{orb}}^{\parallel}$	$P_{\text{WZ}}^{\ddagger\ddagger}$
IR Gem	3.76(8)	15.963(32)	0.538(136)	0.115(4)	0.065(5)	0.06840	0.00(0)
TCP J20100517+1303006	1.87(17)	17.915(21)	0.733(88)	0.338(29)	0.191(41)	—	0.00(0)
CRTS J102705.8-434341	1.43(26)	19.039(61)	0.853(259)	0.212(30)	0.119(41)	0.07800	0.00(0)
GX Cas	2.66(23)	18.264(12)	1.028(74)	0.224(26)	0.127(38)	0.08902	0.00(0)
NSV 14652	1.59(22)	18.376(17)	0.813(75)	0.462(15)	0.262(20)	0.07824	0.00(0)
CC Cnc	1.90(25)	17.433(21)	0.550(91)	0.096(4)	0.054(5)	0.07352	0.00(0)
AD Men	1.83(19)	18.551(15)	0.869(69)	0.161(6)	0.091(8)	0.09170	0.00(0)
V660 Her	1.26(16)	18.559(15)	0.667(78)	0.253(7)	0.142(9)	0.07826	0.00(0)
KS UMa	2.71(11)	16.821(13)	0.587(62)	0.018(0)	0.010(0)	0.06796	0.00(0)
MASTER OT J212624.16+253827.2	1.88(33)	18.635(13)	0.935(60)	0.218(25)	0.123(36)	0.08700	0.00(0)
EI Psc	6.55(7)	15.908(5)	0.904(24)	0.126(1)	0.071(2)	0.04457	0.00(0)
ASASSN-15fv	0.99(15)	18.430(26)	0.469(91)	0.127(4)	0.072(5)	—	0.00(0)
BZ Cir	2.16(7)	17.063(23)	0.610(91)	0.300(13)	0.169(17)	0.07900	0.00(0)
KP Cas	1.79(26)	19.070(17)	1.069(77)	0.283(62)	0.160(92)	—	0.00(0)
V1006 Cyg	2.08(7)	17.287(25)	0.625(105)	0.184(6)	0.104(7)	0.09903	0.00(0)
SS UMi	1.89(5)	16.839(17)	0.438(68)	0.079(1)	0.044(1)	0.06778	0.00(0)
HS Vir	2.84(6)	15.791(16)	0.418(56)	0.117(1)	0.066(1)	0.07690	0.00(0)
NSV 35	4.05(3)	15.111(29)	0.430(151)	0.061(2)	0.034(1)	0.07900	0.00(0)
V444 Peg	2.47(24)	18.641(27)	1.132(151)	0.061(3)	0.034(4)	0.09260	0.00(0)
CRTS J214738.4+244554	2.01(22)	18.363(23)	0.946(105)	0.130(9)	0.073(12)	0.09273	0.00(0)
CRTS J015051.5+332622	1.53(16)	17.787(24)	0.607(103)	0.104(3)	0.059(4)	—	0.00(0)
V632 Cyg	1.95(7)	17.196(21)	0.684(104)	0.428(19)	0.242(25)	0.06377	0.00(0)
QU Aqr	1.06(13)	18.159(13)	0.520(79)	0.187(3)	0.105(3)	0.08330	0.00(0)
V728 CrA	1.72(11)	17.045(20)	0.525(77)	0.258(16)	0.145(22)	—	0.00(0)
ASASSN-15aq	1.61(11)	17.635(20)	0.600(113)	0.038(1)	0.021(1)	—	0.00(0)
V1239 Her	3.40(13)	17.913(25)	1.150(116)	0.041(1)	0.023(2)	0.10008	0.00(0)
DT Oct	3.55(4)	16.223(23)	0.767(93)	0.279(6)	0.157(5)	—	0.00(0)
ASASSN-14eq	1.54(10)	17.743(27)	0.612(113)	0.022(0)	0.012(0)	—	0.00(0)
V1227 Her	1.11(17)	18.079(14)	0.557(59)	0.179(2)	0.100(2)	0.06442	0.00(0)
BF Ara	2.03(23)	18.212(20)	1.015(127)	0.318(40)	0.180(59)	0.08417	0.00(0)
CzeV404	2.94(5)	16.040(42)	0.645(176)	0.335(13)	0.189(12)	0.09802	0.00(0)
1RXS J001538.2+263656	1.64(19)	17.626(23)	0.679(94)	0.081(2)	0.046(2)	0.10150	0.00(0)
ASASSN-13bc	0.91(13)	18.777(39)	0.655(198)	0.086(3)	0.048(2)	—	0.00(0)
ASASSN-15cl	1.86(27)	18.931(15)	1.189(89)	0.245(50)	0.139(75)	—	0.00(0)
BR Lup	1.60(18)	17.758(10)	0.796(48)	0.308(27)	0.174(39)	0.07950	0.00(0)
SDSS J225831.18-094931.7	3.37(6)	15.076(95)	0.445(395)	0.090(6)	0.051(4)	0.08257	0.00(0)
CRTS J155631.0-080440	0.97(19)	18.360(30)	0.708(152)	0.424(12)	0.240(9)	—	0.00(0)
V589 Her	1.01(17)	18.884(36)	0.798(141)	0.127(3)	0.071(2)	—	0.00(0)
ASASSN-15rs	1.77(8)	16.714(51)	0.628(207)	0.441(34)	0.249(43)	—	0.00(0)
DDE 76	1.83(5)	16.144(30)	0.392(133)	0.060(2)	0.033(1)	—	0.00(0)
VZ Pyx	3.98(4)	15.321(32)	0.707(119)	0.207(5)	0.116(5)	0.07332	0.00(0)
SDSS J173008.38+624754.7	1.86(4)	16.417(31)	0.534(152)	0.065(2)	0.037(1)	0.07654	0.00(0)
NY Ser	1.29(5)	16.075(39)	0.225(157)	0.099(3)	0.056(2)	0.09750	0.00(0)
KIS J192254.92+430905.4	0.74(7)	17.214(14)	0.269(66)	0.270(7)	0.151(9)	0.07461	0.00(0)
TU Men	3.60(6)	17.081(13)	1.186(65)	0.165(3)	0.093(3)	0.11720	0.00(0)
NY Her	0.56(9)	18.677(73)	0.520(333)	0.131(8)	0.073(5)	—	0.00(0)
WX Hyi	4.27(3)	14.628(22)	0.668(147)	0.079(2)	0.045(2)	0.07481	0.00(0)
YZ Cnc	4.17(5)	13.988(87)	0.486(393)	0.050(4)	0.028(2)	0.08680	0.00(0)
ASASSN-14kf	2.49(50)	19.664(5)	1.799(71)	0.033(3)	0.020(5)	—	0.00(0)
QZ Ser	3.11(9)	17.245(2)	1.263(23)	0.097(1)	0.055(2)	0.08316	0.00(0)
CSS J221822.9+344511	0.68(12)	17.670(15)	0.509(66)	0.247(4)	0.139(5)	—	0.00(0)
CRTS J203937.7-042908	1.27(15)	17.859(6)	1.064(34)	0.119(3)	0.067(4)	0.10572	0.00(0)
V476 Peg	1.53(6)	16.901(11)	1.223(71)	0.431(13)	0.245(18)	0.06370	0.00(0)